Processing and Application of Ceramics 19 [1] (2025) 94–107
https://doi.org/10.2298/PAC2501094S

Preparation of all solid-state electrolyte lithium ion batteries by multi-layer co-fired process

Derrick Shieh[1], Sea-Fue Wang[1,*], Po-Wei Chi[2], Yung-Fu Hsu[1], Maw Kuen Wu[2]

[1]*Department of Materials and Mineral Resources Engineering, National Taipei University of Technology, Taipei, ROC*
[2]*Institute of Physics, Academia Sinica, Taipei, ROC*

Received 2 January 2025; Received in revised form 18 March 2025; Accepted 23 March 2025

Abstract

This study aims to develop a single-cell prototype of a bulk all-solid-state electrolyte lithium-ion battery (ASSELIB) using the multi-layer co-fired ceramic (MLCC) method. The primary active materials selected for these experiments were as follows: i) solid-state electrolyte material: lithium aluminium titanium phosphate ($Li_{1.3}Al_{0.3}Ti_{1.7}(PO_4)_3$, LATP) with a NaSICON structure, ii) cathode material: lithium nickel cobalt manganese oxide ($LiNi_{0.8}Co_{0.1}Mn_{0.1}O_2$, NCM) and iii) anode material: a mixture of lithium titanium oxide ($Li_4Ti_5O_{12}$, LTO) with a spinel structure and titanium dioxide with a rutile structure (R-TiO_2). The powders of these three components were sequentially layered into a specific mould, forming three distinct layers: cathode, electrolyte and anode. The electrolyte layer was placed between the cathode and anode layers to ensure effective separation and prevent direct contact. The layered sample was then subjected to high pressure, creating a solid laminated bulk structure. At high temperatures, the solid components were co-sintered to form a well-connected interface that allows lithium ions to migrate smoothly across the electrolyte, moving between the cathode and anode. In this study, influences of different composition of ASSELIB layers and different co-fired temperatures (600, 650, 700, 750 and 800 °C) on the performances of the ASSELIB single cell were investigated. The battery's physical properties, density changes and electrochemical characteristics were evaluated, including the formation quality of solid interfaces between each layer, ensuring no chemical interaction between components. Future work will be focused on optimizing the cell by adjusting experimental parameters for enhanced performance.

Keywords: *lithium ion battery, cathode/electrolyte/anode, multi-layer co-fired ceramics, performances*

I. Introduction

Since their inception, lithium-ion batteries have quickly become the world's most popular mainstream product. Enhancing various performance aspects of lithium-ion batteries has therefore become an urgent and essential research focus, especially in extreme environments with significant temperature fluctuations (such as on the Moon, in deep-sea depths and within the Earth's core). The development of the next generation of lithium-ion batteries with solid electrolytes, known as all-solid-state electrolyte lithium-ion battery (ASSELIBs), is emerging as an optimal solution. Solid electrolytes offer notable advantages, such as enhanced safety, no leakage, no need for a separator, non-flammability, operation over a wider temperature range and extremely high energy density, all of which can significantly improve and boost the performance of conventional lithium-ion batteries.

While research on various solid-state battery components has yielded excellent results, progress on effectively bonding these solid components within a battery has been relatively slow, even with high costs preventing commercial-scale production. Therefore, finding an efficient and straightforward mass-production method that can combine three solid-state components cost-effectively remains a crucial challenge for scientists working on solid-state electrolyte lithium batteries.

The multi-layer co-fired ceramic method (MLCC) is a highly feasible approach to bonding two or more ce-

*Corresponding author: +886 22771 2171 #1001
e-mail: *sfwang@ntut.edu.tw*

ramic powders and it has been proven in industrial mass production over many years. This mature technique is primarily used to manufacture multi-layer ceramic capacitors (MLCCs), where dielectric material layers and positive and negative electrode layers are stacked to form a plate capacitor. Connecting the same electrodes of each plate capacitor to an external electrode yields a capacitor with larger total capacitance, thereby increasing the total energy storage. As shown in Fig. 1, a cross-sectional scheme of a single capacitor illustrates that the MLCCs and ASSELIB structures are highly similar. By replacing the dielectric material between the positive and negative electrodes with a solid-state lithium-ion electrolyte, it is possible to create an all-solid-state lithium-ion battery.

Co-firing involves sintering several solid materials together, which imposes very high requirements on the compatibility of their physical and chemical properties. Therefore, a detailed analysis and recording of the physical and chemical properties of each selected solid raw material are necessary, and materials with higher potential for use as electrolyte active materials, anode active materials and cathode active materials should be selected [2].

The preferred active material for solid state electrolyte (SSE) is lithium aluminium titanium phosphate ($Li_{1.3}Al_{0.3}Ti_{1.7}(PO_4)_3$, LATP) [3,4], a compound with a NaSICON-type structure. LATP has a good conductivity (10^{-4}–10^{-3} S/cm), excellent thermal and mechanical stability, lower sintering temperature and most importantly good environmental stability [5], allowing it to be stored and used at normal room temperature. Thus, in this work undoped LATP as the preferred active SSE material was used.

The best choice for anode is a mixture of rutile structured titanium dioxide (R-TiO_2) [6] and $Li_4Ti_5O_{12}$ (LTO) [7] in a specific ratio as the anode active material. This mixture is not only suitable for general laboratory operations, but also unexpectedly yields better anode performance than bare LTO, making the LTO + R-TiO_2 mixed anode our preferred choice.

Attractive cathode material is lithium nickel cobalt manganese oxide with a layered structure, $LiNi_{0.8}Co_{0.1}Mn_{0.1}O_2$ (NCM) [8–10], which is widely used due to its high energy density and easy availability as a cathode active material.

For the conductive material, carbon [11–16] is used at a low sintering temperature of 600 °C. Glucose is a good carbon source which was mixed into the composite electrode material, leaving carbon as a conductive material after heat treatment, forming a carbon-coated electrode. When sintering at higher temperatures (≥ 800 °C) is performed, copper metal is used as the conductive material [17]. This is achieved by mixing copper oxide (CuO) and glucose into the composite electrode material, where a displacement reaction occurs after high-temperature heat treatment to yield metallic copper, as shown in Eq. 1:

$$2\,CuO + C \longrightarrow 2Cu + CO_2 \qquad (1)$$

When using the displacement reaction in Eq. 1 to obtain copper metal as a conductive material, it is essential to maintain a 1:1 mole ratio of Cu to C, so the weight ratio of CuO to glucose is precisely 1:2.

For the co-sintered solder, lithium borate $Li_{2.6}BO_3$, specifically Al-doped compound $Li_{2.6-x}Al_xBO_3$ (LABO), was used as the preferred option [18–20].

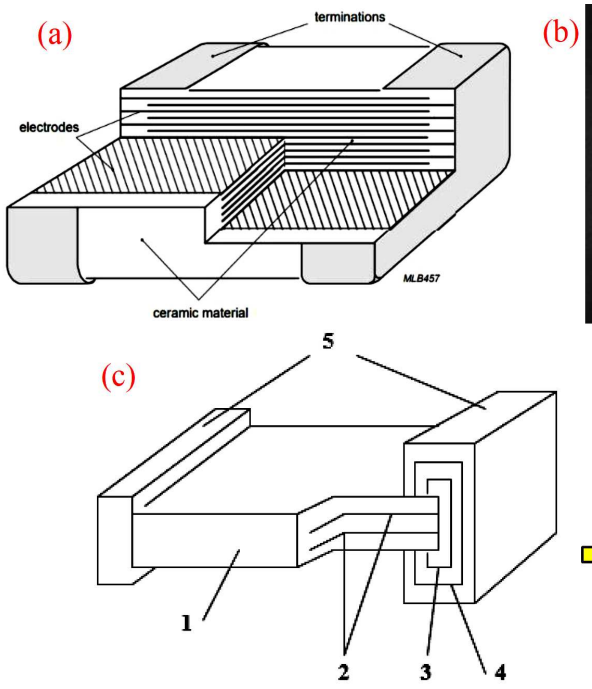

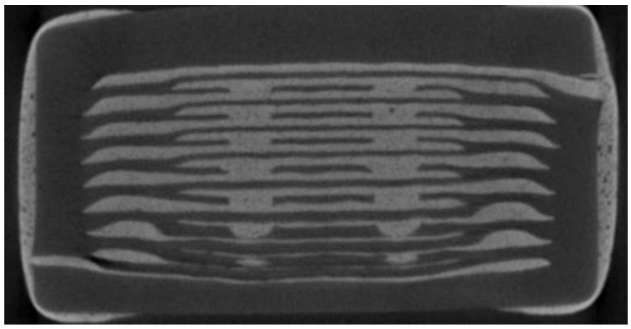

No	Parts	Process
1	dielectric material	co-fired
2	internal electrode	co-fired
3	Termination electrode	co-fired
4	1st electroplating layer	post-work
5	2nd electroplating layer	post-work

Figure 1. Cross-sectional view (a), 3D X-ray CT of the laminated finished MLCC product [1] (b) and cross-sectional schematic illustration of a plate-capacitor (c)

Table 1. The basic components and their functions in ASSELIBs

Cell parts	Active material	Additive material	Conductive material	Adhesive
Positive electrode	NCM811	LATP	CuO + glucose	LABO
Solid electrolyte	LAPT	Glucose	-	LABO
Negative electrode	R-TiO_2 + LTO	LATP	CuO + glucose	LABO

The main reason for choosing LABO is its low melting point, allowing it to be consumed during processing. It does not remain in the battery due to the low melting point of 590–600 °C. In addition, it does not easily react with other active materials in the battery, provides excellent metal oxide solderability, has effective sintering additive properties and also helps to inhibit side reactions at interfaces.

Regarding the binder for the pressing process, polyvinyl alcohol (PVA), a commonly used binder in ceramic sintering was selected. PVA is easily consumed during the debinding process due to its low thermal stability, beginning to decompose at 200–250 °C, forming a six-membered ring transitional state and undergoing random cleavage to produce acetaldehyde, unsaturated aldehydes, ketones and other compounds. Upon further heating to 500 °C, all remaining organic material volatilizes without leaving residues in the battery.

All of the preferred battery component materials given above should not undergo chemical reactions with each other at the sintering temperatures. The interface can be observed after sintering through XRD diffraction analysis and SEM BSI composition analysis. In this study, we employed a multilayer co-fired method to connect solid particles from different layers at high temperatures, creating a well-connected solid interface that facilitates lithium-ion migration between the cathode and anode, enabling the successful fabrication of an all-solid-state electrolyte lithium-ion single cell battery without compromising any of the components.

For optimizing the composition ratio of co-sintered solid-state battery components, our strategy was first to determine the solid electrolyte composition ratio through simple multilayer co-sintering experiments as the foundation for all optimizations. Then we fabricated the battery and measured its performance at different sintering temperatures, gradually optimizing the anode composition ratio, followed by the final adjustments to optimize the cathode composition ratio.

II. Experimental

The ASSELIBs are basically composed of materials with different functions [21]:

1. Positive electrode (cathode): includes positive active materials, additives, conductive materials and adhesive add.
2. Electrolyte: includes electrolyte active materials and adhesive add.
3. Negative electrode (anode): includes negative electrode active materials, additives, conductive materials and adhesive add.

The components used in this experiment and their uses are shown in Table 1.

All materials used for fabrication of the ASSELIB cells were self-manufactured in our laboratory and only lithium nickel cobalt manganese oxide ($LiNi_{0.8}Co_{0.1}Mn_{0.1}O_2$) and titanium dioxide ($TiO_2$) were commercial. $LiNi_{0.8}Co_{0.1}Mn_{0.1}O_2$ with a layered structure (product NCM811) was manufactured by UBIQ Technology Co, Ltd. and anatase TiO_2 powder was purchased from Showa Chemical.

2.1. Solid state electrolyte (SSE)

Electrolytes for the ASSELIB cells were prepared from $Li_{1.3}Al_{0.3}Ti_{1.7}(PO_4)_3$ (LATP) with different amount of lithium aluminium borate ($Li_{2.6-x}Al_xBO_3$, LABO). The LATP powder was prepared using the solid synthesis method [22]. The raw materials, including aluminium oxide (Al_2O_3), titanium dioxide (TiO_2), ammonium dihydrogen phosphate ($NH_4H_2PO_4$) and an excess of lithium hydroxide ($LiOH \cdot H_2O$), were mixed in stoichiometric ratio. This mixture was placed in a ball mill jar containing zirconia balls and isopropanol solvent and milled for 20 h. After milling, the slurry was dried in an oven at 90 °C for 24 h. The dried powder was ground uniformly in a mortar, placed in a crucible and calcined at 900 °C for 4 h with a heating/cooling rate of 5 °C/min to form the LATP phase. To reduce powder agglomeration after calcination, a second wet ball milling for 12 h was necessary. The obtained powder was dried at 90 °C for 24 h and then sieved through a 200-mesh screen to control the particle size, thus completing the preparation of the LATP calcined powder.

The solder material LABO was prepared using the solid synthesis method [23]. The raw materials, including boric acid (H_3BO_3), aluminium oxide (Al_2O_3) and an excess of $LiOH \cdot H_2O$, were mixed according to stoichiometry and ball-milled with zirconia balls and isopropanol for 20 h. After milling, the zirconia balls were taken out and the slurry was dried in an oven at 90 °C for 24 h. The dried powder was ground, placed in a crucible and calcined at 570 °C for 2 h with a heating/cooling rate of 5 °C/min to form the LABO phase structure. A second wet ball milling for 12 h was performed, followed by drying and sieving through a 200-mesh screen to control the particle size, completing the preparation of the LABO calcined powder.

2.2. Electrodes for ASSELIB cells

The anode active materials, based on lithium titanate ($Li_4Ti_5O_{12}$, LTO) with a spinel structure, were prepared using the solid synthesis method [24]. The raw materials, including TiO_2 and an excess of $LiOH \cdot H_2O$, were

mixed according to stoichiometry and ball-milled with zirconia balls and isopropanol for 20 h. After milling, the slurry was dried in an oven at 90 °C for 24 h. The dried powder was ground in a mortar, placed in a crucible and calcined at 800 °C for 2 h with a heating/cooling rate of 5 °C/min to form the LTO phase structure. A second wet ball milling for 12 h was performed to reduce powder agglomeration, followed by drying and sieving through a 200-mesh screen to control the particle size, completing the preparation of the LTO calcined powder. Different anode active materials were examined, i.e. LTO was mixed with different amount of TiO_2 and glucose. The rutile (R-TiO_2) powder for anode material was prepared by converting commercial anatase TiO_2 to rutile TiO_2 by heating to above 750 °C for 4 h.

Different cathode active materials were obtained by using the commercial $LiNi_{0.8}Co_{0.1}Mn_{0.1}O_2$ (NCM) with 5, 10, 20 and 30 wt.% of LATP.

2.3. *Fabrication of co-fired ASSELIB cells*

The ASSELIB cells were fabricated in a few steps [25]. From Fig. 2, it can be seen that the first half of the pelletizing method is exactly the same as tape casting. The only difference is that the mould lamination process (multi-layer pelletizing) in the later stage is changed to the slurry-preparation and the tape lamination process, which will takes 5 more days.

2.4. *Structural and electrochemical characterization*

X-ray diffraction (XRD) analysis was performed using a Bruker D2 Phaser A26-X1-A2B0B2A diffractometer to identify the crystalline phases of the prepared powders. The X-ray source was CuKα (0.15418 Å), with a 0.6 mm filter slit, operating at 30 kV and 10 mA. The scan rate was 1 °/min with a step size of 0.02°, covering a 2θ range of 10–60°. The diffraction patterns were analysed using HighScore Plus software and the lattice constants were calculated using Bruker's TOPAS software with Rietveld refinement.

Scanning electron microscopy (SEM) analysis was performed using a JEOL LSM-6510LV thermal field emission microscope to observe the surface and cross-sectional microstructures of the samples. The samples were mounted on conductive carbon tape and gold-coated to enhance conductivity and prevent charge accumulation during SEM observation. The operating conditions were 15 kV acceleration voltage and 10 mA current. SEI mode was used to observe the micro-structure, BEI composition mode for element mapping and interface observation, and BEI topography mode for surface topology.

Density measurement was conducted using the Archimedes method with isopropanol as the liquid medium. The absolute density values were referenced from publicly available data and the relative density of the samples was calculated.

Electrochemical impedance spectroscopy (EIS) measurements were conducted using a Solartron 1470E. The frequency range was 1 MHz to 5 kHz. The impedance data were analysed using Zview software, fitting the data to an equivalent circuit model consisting of a series of a resistor (R) and two circuits having parallel constant phase elements (CPE) and resistor components (inset in Fig. 3e). The high-frequency component represented the total material impedance and the low-frequency component represented the contact impedance.

The ASSELIB single cell electrochemical performance was tested using the aforementioned EIS setup. Charge-discharge cycles and capacity measurements were performed to evaluate the cells' performance under different composition ratios and sintering temperatures.

III. Results and discussion

3.1. *Optimal composition of ASSELIB components*

The MLCC method involves stacking several solid raw materials to form a multilayer block which is then sintered simultaneously. This method demands high

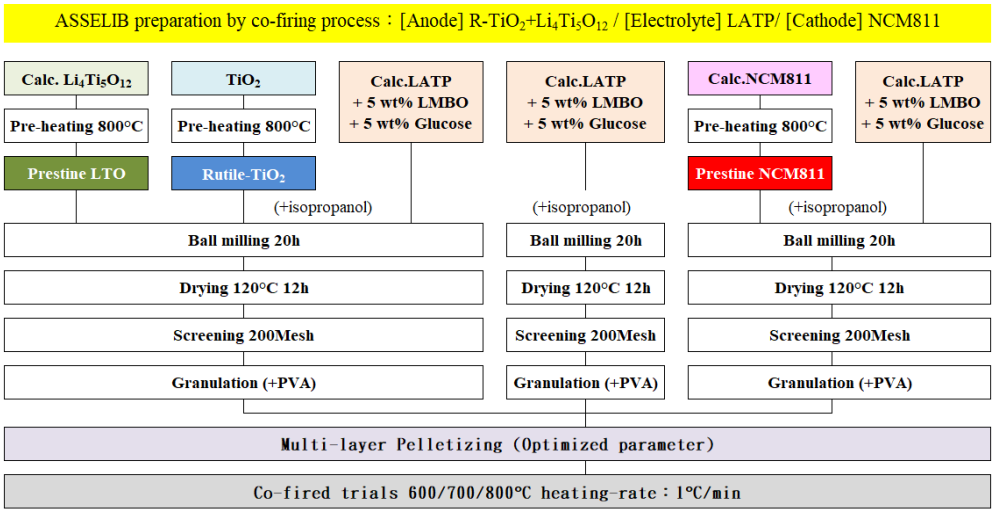

Figure 2. Simple flow chart for the preparation of ASSELIB by co-firing process

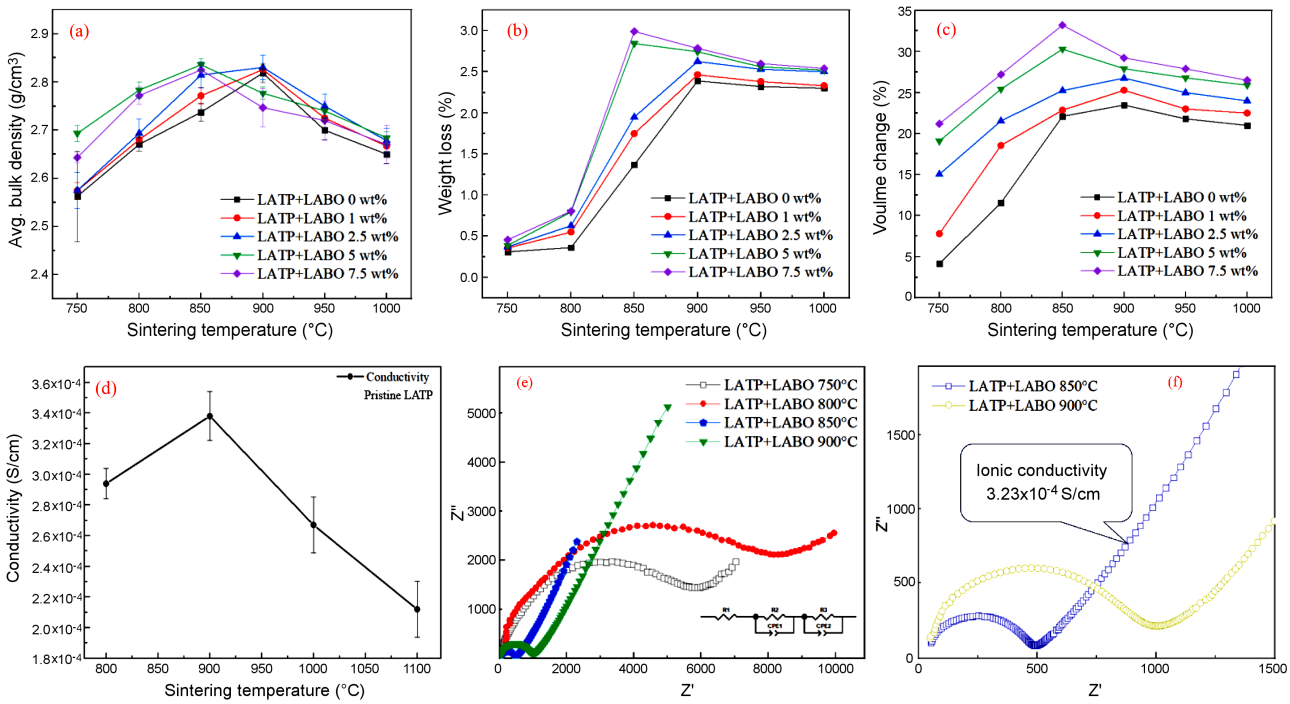

Figure 3. Sintering curve of LATP + *x* wt.% LABO (a), thermogravimetric loss of LATP + *x* wt.% LABO (b), volume change of LATP + *x* wt.% LABO (c), conductivity measurement of pure LATP (d), impedance measurement of LATP + 5 wt.% LABO at different temperatures (e,f)

compatibility in terms of changes in sintering density, thermogravimetric loss, volume changes, melting points and chemical reactions between the raw materials. The following sections discuss the compatibility of physical properties through experimental investigation.

Solid state electrolyte

First, we observed and measured the changes in sintering density, thermogravimetric loss and volume changes of the electrolyte active material (mixtures of LATP with different amounts of LABO) at different temperatures. Thus, the highest density of the pure LATP (bare LATP sample) appeared at 900 °C (Fig. 3a). When LABO was added in amount of 1 and 2.5 wt.%, the highest density still occurs at the same sintering temperature, i.e. 900 °C. However, with further increase of LABO content (5 and 7.5 wt.%) the optimal sintering conditions are at lower temperature, i.e. 850 °C. That indicates that LABO not only acted as an excellent solder, but also showed sintering aid effects. The maximal density corresponded with maximum thermogravimetric loss and volume change (Figs. 3b,c) [26].

As shown in Fig. 3d, the highest ionic conductivity (3.39×10^{-4} S/cm) of the bare LATP was obtained for the sample sintered at 900 °C, and corresponds to the sample having the highest density. We believe that beyond 900 °C, excessive grain growth leads to a decrease in both relative density and conductivity, demonstrating a positive correlation between relative density and conductivity of the SSE. In addition, impedance measurements confirmed high conductivities of the samples LATP + 5 wt.% LABO sintered at 850 and 900 °C (Figs. 3e,f). Thus, from these results, the LATP + 5 wt.% LABO was used as the solid electrolyte active material in the following experiments.

Anode

The changes in density, thermogravimetric loss and volume changes of the mixed anode active materials R-TiO_2 + *x* wt.% LTO at different sintering temperatures were measured too (Fig. 4). The theoretical density of the pristine LTO is 3.54 g/cm^3, and the highest absolute density of 2.76 g/cm^3 was achieved after sintering at 850 °C for 4 h (Fig. 4a). However, for the mixed anode R-TiO_2 + 5 wt.% LTO the best absolute density of 3.85 g/cm^3 was achieved after sintering at 900 °C for 2 h (Fig. 4b) and minimal changes in thermogravimetric loss and volume were obtained above 900 °C (Fig. 4c). It means that the optimal sintering temperature could be 900 °C.

Cathode

The sintering density, thermogravimetric loss and volume changes of the composite NCM cathode at different temperatures [27] were analysed, as shown in Fig. 5. The NCM has theoretical density [28] of 4.81 g/cm^3 and a layered structure at low temperature. When the temperature rises to 900 °C, lithium vacancies occur due to Li^+ loss. These vacancies are easily occupied by Ni^{2+} ions with a radius close to Li^+, leading to a structural transformation into a rock-salt or spinel structure with poor lithium ion migration. Figure 5a clearly shows significant density changes between 800–900 °C, indicating a phase transition in the NCM structure. High slopes

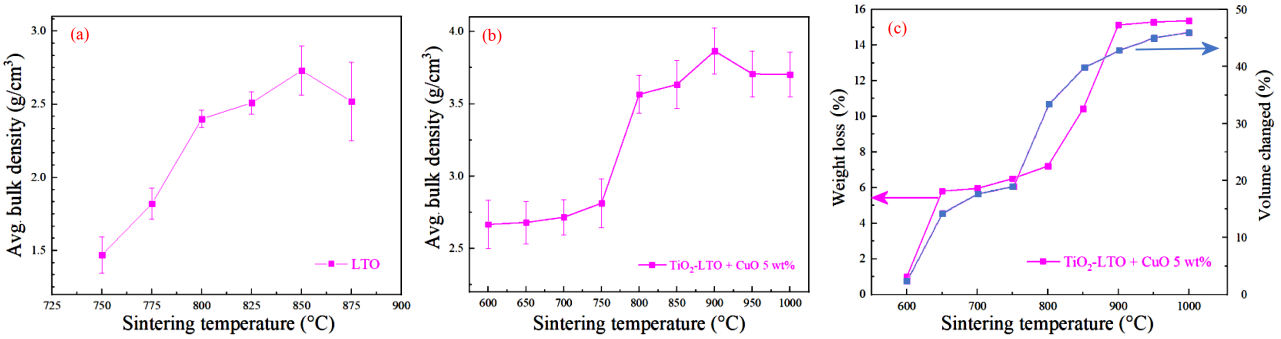

Figure 4. Sintering curves of bare LTO (a) and mixed anode R-TiO_2 + 5 wt.% LTO + 5 wt.% CuO samples (b) as well as thermogravimetric loss and volume change curves of mixed anode R-TiO_2 + 5 wt.% LTO + 5 wt.% CuO sample

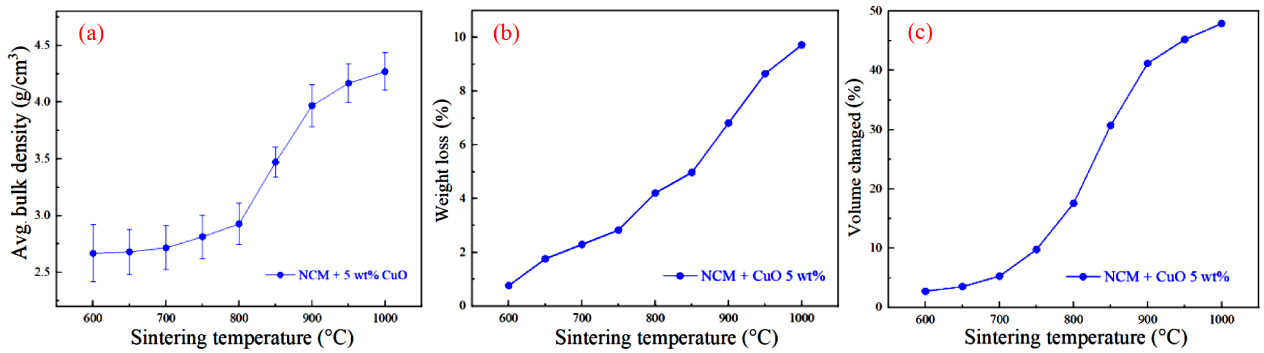

Figure 5. Sintering (a), thermogravimetric loss (b) and volume change (c) curves of NCM composite cathode

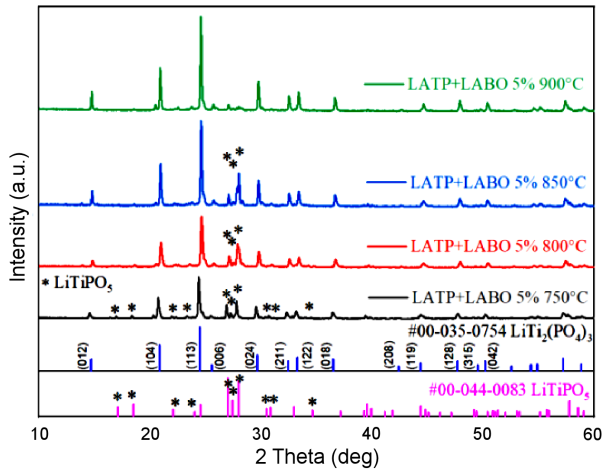

Figure 6. XRD pattern of LATP + 5 wt.% LABO mixture sintered at 700, 800, 900 and 1000 °C for 2 h

in thermogravimetric loss (Fig. 5b) and the volume change (Fig. 5c) in temperature range between 800–900 °C can be additional evidence of the phase transition. Referencing the experimental results of Yue *et al.* [29], it was found that sintering at 850 °C yields the best performance for the cathode material, which is very similar to the results of this study.

3.2. Chemical compatibility of ASSELIB components

In the next step, possible interaction between LATP and LABO (used for electrolyte fabrication) was analysed. Thus, for the SSE composite, the bare mixture of LATP + 5 wt.% LABO was sintered at 750, 800, 850 and 900 °C for 2 h. XRD analyses presented in Fig. 6 shows no chemical reaction between LATP and LABO. The main reason is low melting point of LABO, being approximately 575 °C, causing that this compound did not remain in the mixture at high temperature. At the same time Hupfer *et al.* [30] mentioned that the secondary $LiTiPO_5$ phase was formed while preparing LATP by solid synthesis method, what was also observed in our work (Fig. 6).

Cathode

To analyse chemical compatibility of cathode with electrolyte materials, the NCM and LATP powders were mixed in a mass ratio of 50:50 and heated to 800 °C/2 h. XRD analysis of the resulting mixture (Fig. 7) revealed a chemical reaction between NCM and LATP. However, when the LATP amount was decreased to 5 wt.% no reaction occurred even when temperature was increased to 1000 °C (Fig. 8a). From these experiments, it is evident that LATP as a filler does not affect the operation of the NCM cathode active material while LATP content is below 5 wt.% [9].

In addition, pristine mixture of LATP with 5 wt.% NCM was sintered at 750, 800, 850 and 900 °C for 2 h. The XRD analysis of the resulting mixtures (Fig. 8b) indicated that no reaction occurred between the two materials. This experiment shows that when LATP comes into contact with a small amount of NCM cathode material at the solid-state interface it should not affect the performance of the LATP electrolyte material.

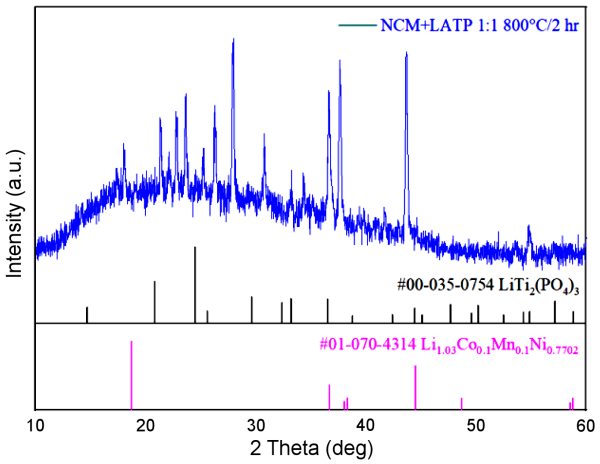

Figure 7. XRD pattern of bare NCM + LATP mixture with mass ratio 50:50 sintered at 800 °C/2 h

Anode

To analyse chemical compatibility of anode with electrolyte materials, the LTO and LATP powders were mixed in a mass ration 50:50 and heated to 800 °C/2 h. XRD analysis of the resulting mixture in Fig. 9a revealed a chemical reaction between LTO and LATP. However, when the LATP content was decreased to 5 wt.% no reaction occurred even when the temperature increased to 1000 °C (Fig. 9b).

In addition, the effect of 3, 5 and 7 wt.% glucose in the LTO + 5 wt.% LATP sample sintered at 800 °C/2 h was also investigated. It is evident from Fig. 9c that no reaction occurred even when the temperature increased to 1000 °C. Thus, it can be concluded that LATP (as well as LATP/glucose) as a filler does not affect the operation of the LTO anode active material.

3.3. *Structure and performances of ASSELIB*

The first step in experimental strategy for fabrication of the co-fired ASSELIB cells (all-solid-state electrolyte lithium-ion battery) was to confirm the compositions of the SSE components, then to adjust the composition of the negative electrode components and finally to optimize the composition of the positive electrode and complete the entire ASSELIB. The second step in strategy was to select optimal sintering temperature [31].

From the results presented in section 3.1, it can be concluded that the optimal sintering temperature for the mixed electrolyte active material is 800 °C/2 h; for the mixed anode active material R-TiO_2 + LTO it is 900 °C/2 h; and for the mixed cathode active material NCM + LATP, it is 850 °C/2 h. Theoretically, increasing the density of the electrolyte component helps improve lithium-ion conductivity. However, high density of the anode and cathode materials is harmful to lithium-ion lithiation and delithiation [32]. Therefore, we decided

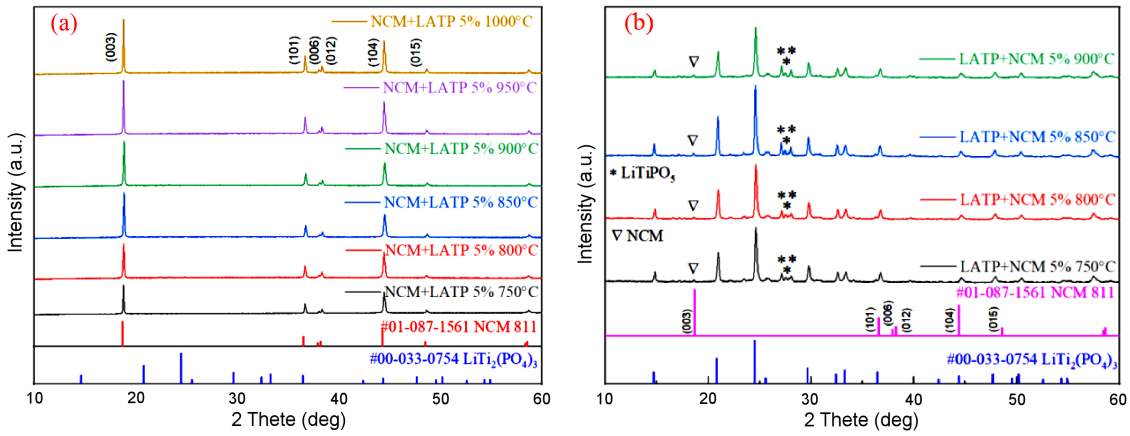

Figure 8. XRD patterns of: a) NCM with 5 wt.% LATP and b) LATP with 5 wt.% NCM mixtures, sintered at 750, 800, 850, 900, 950 and 1000 °C for 2 h

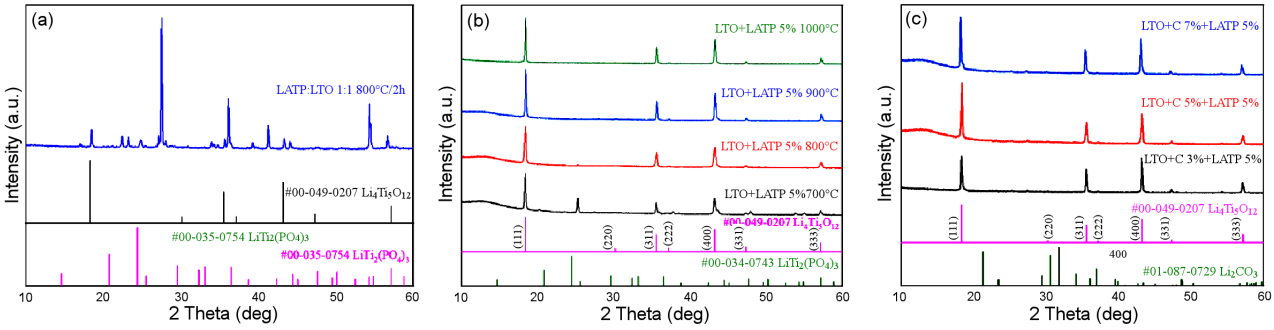

Figure 9. XRD patterns of: a) LTO + LATP mixture with 50:50 wt.% ratio sintered at 800 °C/2 h, b) LTO with 5 wt.% LATP sintered at 700, 800, 900 and 1000 °C for 2 h and c) LTO + LATP mixture with glucose content of 3, 5 and 7 wt.% sintered at 800 °C/2 h

to use a target sintering temperature of 800 °C/2 h, aiming for optimal electrolyte density while achieving relatively high density for both anode and cathode components.

To reach the target sintering temperature of 800 °C/2 h, we considered two possible issues: first, the release of CO_2 due to the thermal reactions involving carbon elements, and second, potential battery cracking caused by differences in volume changes among layers during high-temperature co-sintering. To address the first issue, we opted to use metallic copper as the conductive material instead of carbon, as copper can eliminate CO_2 formation. For the second issue, we examined the thermogravimetric loss and thermal expansion of each component and found that the cathode component is more sensitive to high-temperature changes, showing significant differences at 800 °C/2 h. Thus, we decided to adjust the composition ratio or other parameters of the cathode component to align with the thermal volume changes of the LATP solid electrolyte.

Structure of co-fired ASSELIB

In the co-fired ASSELIB structure [33–36], in order to ensure close contact between the electrode and the electrolyte, we mixed electrolyte particles into the electrode, as shown in Fig. 10.

The co-fired ASSELIB cells fabricated with LATP + 5 wt.% LABO as the active material for the SSE are shown in Fig. 11. Clear cracks can be observed at the surface of the ASSELIB prepared without carbon in the bare LATP, labelled as B1 (Fig. 11a). However, no surface defects were observed in the ASSELIB prepared using LATP with added carbon under the same conditions, labelled as B2 (Fig. 11b).

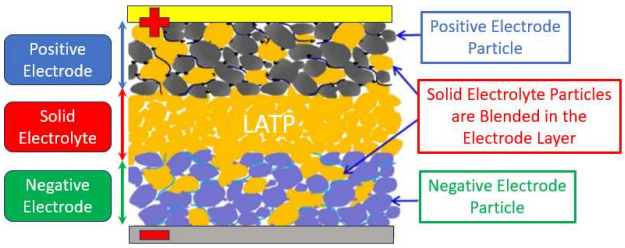

Figure 10. Schematic presentation of the ASSELIB cell

SEM was used to examine the interface profiles of the B2 cell cross-section. We found that at both the anode interface (Fig. 12a,b) and the cathode interface (Fig. 12c,d), the solid-state connecting-area has very good bonding, with minimal porosity. In contrast, SEM images of the B1 cell showed loose bonding with a high porosity, as seen in Fig. 13a,b at the anode side and Fig. 13c,d at the cathode side, with the NCM layer exhibiting an irregular structure. These results indicate that the addition of carbon to LATP has a positive impact on the interface during co-firing, acting as a binder. Therefore, the preferred composition of the solid-state electrolyte element in this experiment is LATP + LABO + carbon [37,38].

SEM cross-sectional image obtained by the secondary (SEI) electron mode (Fig. 14a) shows that the interface between components is not clearly defined. In addition, SEM cross-sectional image obtained by the backscattered (BEI) electron mode (Fig. 14b) allows clear identification of each layer's actual thickness at the interfaces. Since lithium ions conduct through diffusion in the solid electrolyte, the thickness of the electrolyte layer greatly influences lithium-ion migration. Due to the limitations of experimental equipment and moulds in the pelletizing process, the minimum thickness of the LATP electrolyte layer was about 600–800 μm, as shown in (Fig. 14b). Also, the thickness of the cathode layer was about 300–320 μm [39,40].

Influence of electrolyte thickness

To understand the impact of electrolyte layer thickness on the solid-state battery performance, we fabricated solid-state batteries with four different electrolyte layer thicknesses: 1.2, 1.0, 0.9 and 0.8 mm, and measured their *C-V* characteristics [41].

Figure 15a shows the *C-V* curve of a conventional liquid lithium battery, where Segment 0 spans from circuit initiation to the end of the first reduction peak, with the peak value representing the initial current peak. Segment 1 extends from the first oxidation peak to the end of the second reduction peak, where the difference between the first and the second reduction peak indicates lithium ion consumption forming the SEI layer. Segment 2 covers the period from the second oxidation peak to the end of the third reduction peak, and so on.

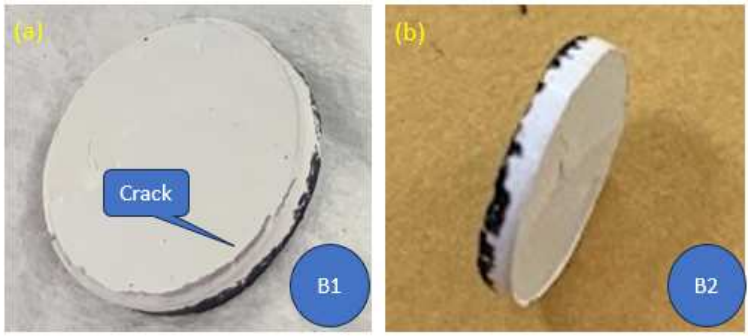

Figure 11. Images of: a) ASSELIB prepared without carbon in LATP (sample B1) and b) ASSELIB containing carbon in LATP (sample B2) after co-firing

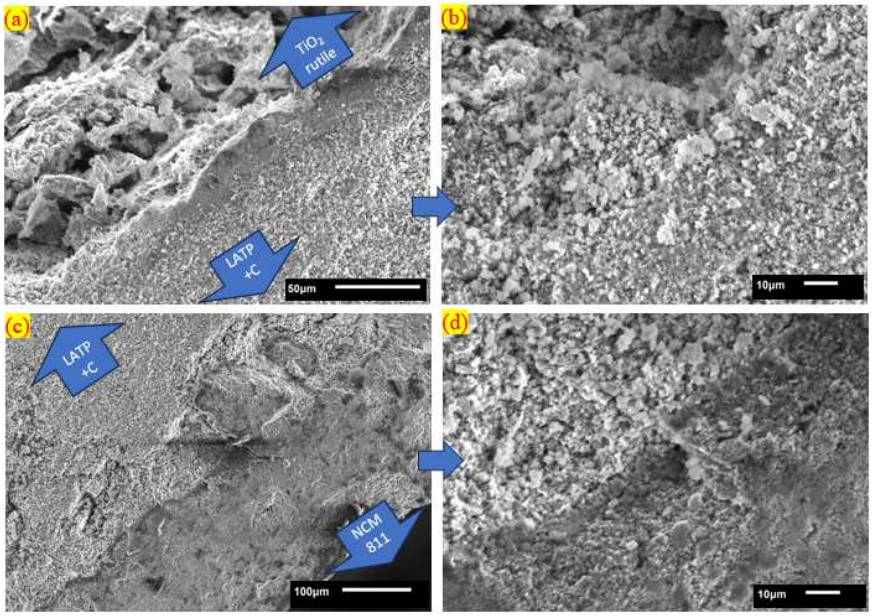

Figure 12. SEM images of ASSELIB-B2 showing interface with: (a,b) negative and (c,d) positive electrode

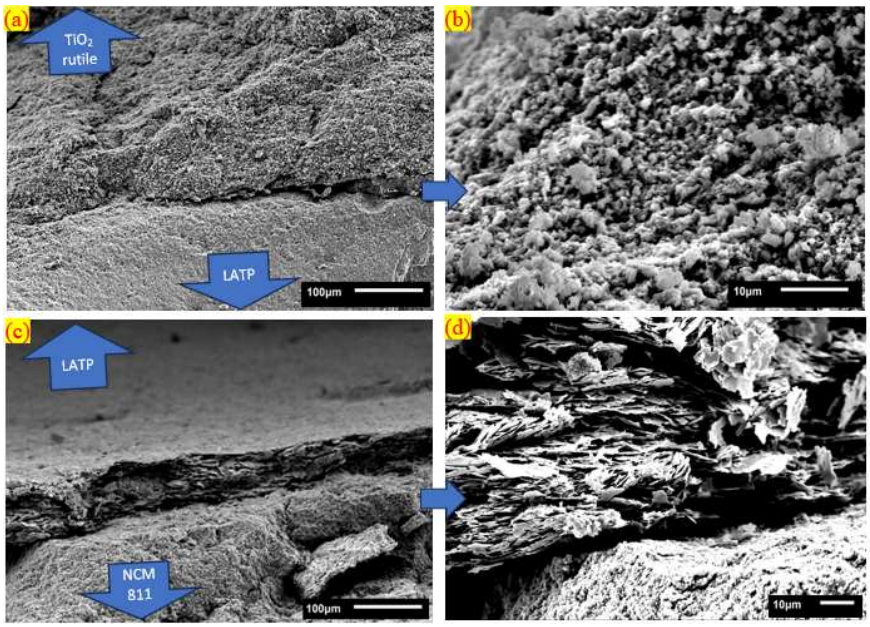

Figure 13. SEM images of ASSELIB-B1 showing interface with: (a,b) negative and (c,d) positive electrode

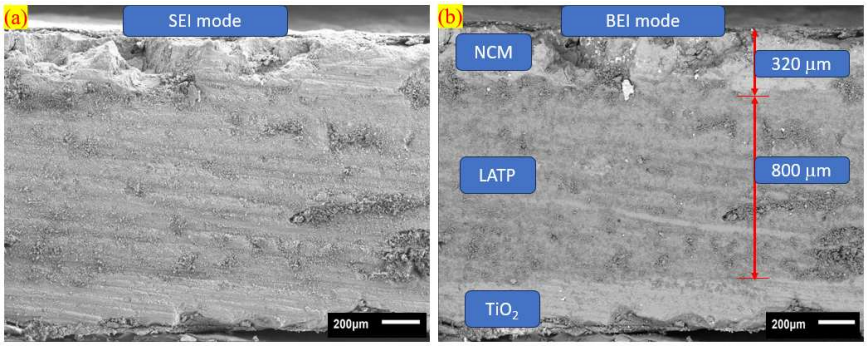

Figure 14. SEM images of ASSELIB-B2 in: a) SEI mode profile and b) BEI mode profile

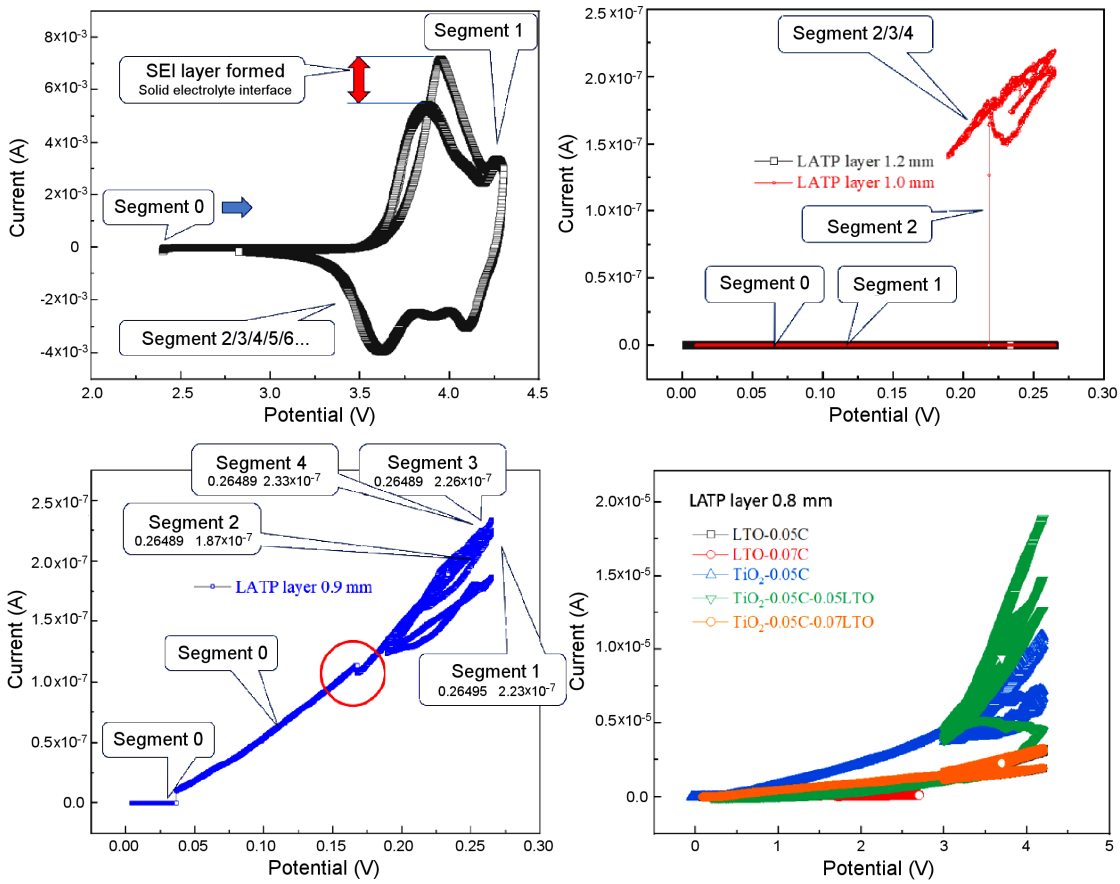

Figure 15. *C-V* plots for: a) typical liquid lithium battery, b) solid-state batteries with 1.2 and 1.0 mm thick electrolyte layers, c) solid-state battery with a 0.9 mm thick electrolyte layer and d) solid-state batteries with 0.8 mm thick electrolyte layers, demonstrating better lithium-ion migration through the thinner electrolyte layer

Figure 15b presents the *C-V* curves of the solid-state lithium batteries with two different electrolyte thicknesses. The *C-V* curve for the black line, representing the 1.2 mm thick electrolyte layer, shows a current value of 0, indicating no lithium-ion migration and thus not pursued further in research. The red curve, for the 1.0 mm thick electrolyte layer, shows current values of 0 in Segments 0 and 1, with a current signal only emerging in Segment 2, indicating significant difficulty for lithium ions to penetrate the electrolyte layer.

Figure 15c displays the *C-V* curve of the 0.9 mm thick electrolyte layer, where current is initially absent at the beginning of Segment 0, but appears shortly after, with a noticeable current step difference at the transition to Segment 1 before continuing to the maximum current. This suggests that lithium ions still struggle to penetrate the 0.9 mm thick electrolyte layer immediately.

Figure 15d shows *C-V* measurements of the solid-state batteries with five different anode components, all with an electrolyte layer thickness of 0.8 mm. The results indicate that all types exhibit an initial current in Segment 0, with the initial current value significantly higher than previously measured, suggesting that lithium ions can penetrate the 0.8 mm thick electrolyte layer barrier almost immediately. Based on these results, we can reasonably infer that adopting a tape casting process to control electrolyte layer thickness between 0.02 and 0.05 mm would greatly enhance electrochemical performance.

Influence of anode composition

Three different types of anode active materials co-fired at 600 °C for 2 h were prepared for solid-state lithium batteries: i) bare LTO + 5 wt.% glucose, ii) bare LTO + 7 wt.% glucose and iii) bare R-TiO_2 + 5 wt.% glucose. The *C-V* measurements, shown in Fig. 16a, indicate that the highest initial current was achieved with the bare R-TiO_2 + 5 wt.% glucose, while the lowest initial current was obtained with the bare LTO + 7 wt.% glucose as the anode material. From these results, we identify the bare R-TiO_2 + 5 wt.% glucose as the preferred anode material in this experiment.

In addition, two additional types of solid-state lithium batteries with different anode active materials (R-TiO_2 + 5 wt.% LTO + 5 wt.% glucose and R-TiO_2 + 7 wt.% LTO + 5 wt.% glucose) were prepared also at 600 °C for 2 h, and their properties were measured for comparison. The results, shown in Fig. 16b, indicate that the highest initial current was achieved with the mixed R-TiO_2 + 5 wt.% LTO + 5 wt.% glucose anode material. When using R-TiO_2 + 7 wt.% LTO + 5 wt.% glucose as the anode, the initial current was the lowest. Based on these

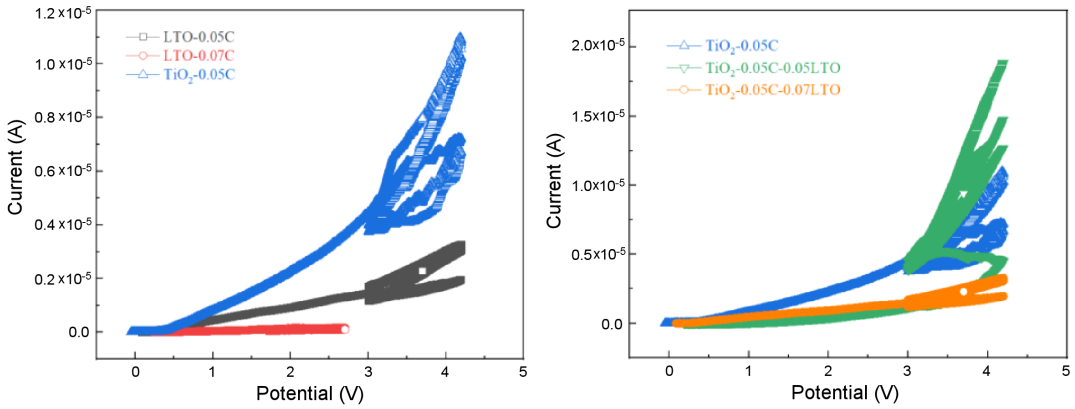

Figure 16. *C-V* graphs for ASSELIB with different anode compositions: a) LTO + 5 wt.% glucose, LTO + 7 wt.% glucose, R-TiO_2 + 5 wt.% glucose and b) R-TiO_2 + 5 wt.% glucose, R-TiO_2 + 5 wt.% LTO + 5 wt.% glucose, R-TiO_2 + 7 wt.% LTO + 5 wt.% glucose

results, the selected preferred anode active material was the R-TiO_2 + 5 wt.% LTO + 5 wt.% glucose mixture.

Influence of cathode composition

Table 2 summarizes the composition of the ASSELIB mixtures and their co-sintering results. Solid-state batteries with different cathode composition were fabricated, i.e. NCM with 5, 10, 20 and 30 wt.% of LATP. It was found that the battery with NCM + 5 wt.% LATP, maintained good appearance after co-sintering at 600, 700 and 750 °C, but at 800 °C the cathode and electrolyte layers separated and split, while the anode layer remained well adhered. With the increase of LATP content in the cathode mixture to 10 and 20 wt.%, separation from the electrolyte was also observed, but surface smoothness was slightly improved. However, significant improvements in the interface between the cathode and electrolyte, as well as high smoothness and good adhesion of the anode layer, was observed in the solid-state battery co-sintered at 800 °C with NCM + 30 wt.% LATP, where the cathode layer thickness was 0.6 mm. Unfortunately, several arc-shaped cracks appeared along the edge of the cathode disc. Subsequently, we fabricated a similar battery with 30 wt.% LATP, increasing the cathode layer thickness to 1.0 mm. After co-sintering at 800 °C, the cathode and electrolyte interface showed well-aligned bonding and the anode layer also exhibited good adhesion with no visible cracks [42].

Based on these results, we conclude that the optimized cathode composition co-fired at 800 °C is NCM + 30 wt.% LATP with an increased cathode thickness. This confirms that adjusting the filler proportion and electrode layer thickness is an effective strategy.

ASSELIB co-firing at different temperatures

The ASSELIB cell composes of the LATP layer separating the cathode and anode to prevent short circuits (Fig. 10). Thus, LATP serves dual functions as both an electrolyte and filler. To minimize differences in thermal expansion between the cathode, electrolyte and anode after co-sintering, while keeping adjustments to the component mixtures minimal, we attempted to increase the proportion of LATP in the electrode mixtures or alter the thickness of the electrode layers. Four different co-fired temperatures (650, 700, 750 and 800 °C for 2 h) were examined.

ASSELIB with different densities were obtained at various sintering temperatures and *C-V* measurements were used to assess the impact of density differences on battery performance. Figure 17 shows the *C-V* curves for the ASSELIB at different co-sintering tempera-

Table 2. Summary table of ASSELIB co-sintering results and component proportions

Cell parts	Code	Composite-composition								Glucose : CuO (mol%= 50:50)		Pelletizing	Co-fired results at 600~750°C	Co-fired results at 800°C
		NCM811 (wt.%)	LATP (wt.%)	R-TiO_2 (wt.%)	LTO (wt.%)	LABO (wt.%)	Glucose (wt.%)	CuO (wt.%)		Glucose (wt.%)		PVA (wt.%)		
Positive electrode	A1	85	5	-	-	5	-	5	+	10	+	5	OK	Bending NG
	A2	80	10	-	-	5	-	5	+	10	+		-	Bending NG
	A3	70	20	-	-	5	-	5	+	10	+		-	Bending NG
	A4	60	30	-	-	5	-	5	+	10	+		-	Better but crack NG
	A5	60	30	-	-	5	-	5	+	10	+		-	Flating OK
Solid electrolyte	B2	-	90	-	-	5	5	-		-	+	5		
Negative electrode	C6	-	5	80	5	5	-	5	+	10	+	5		

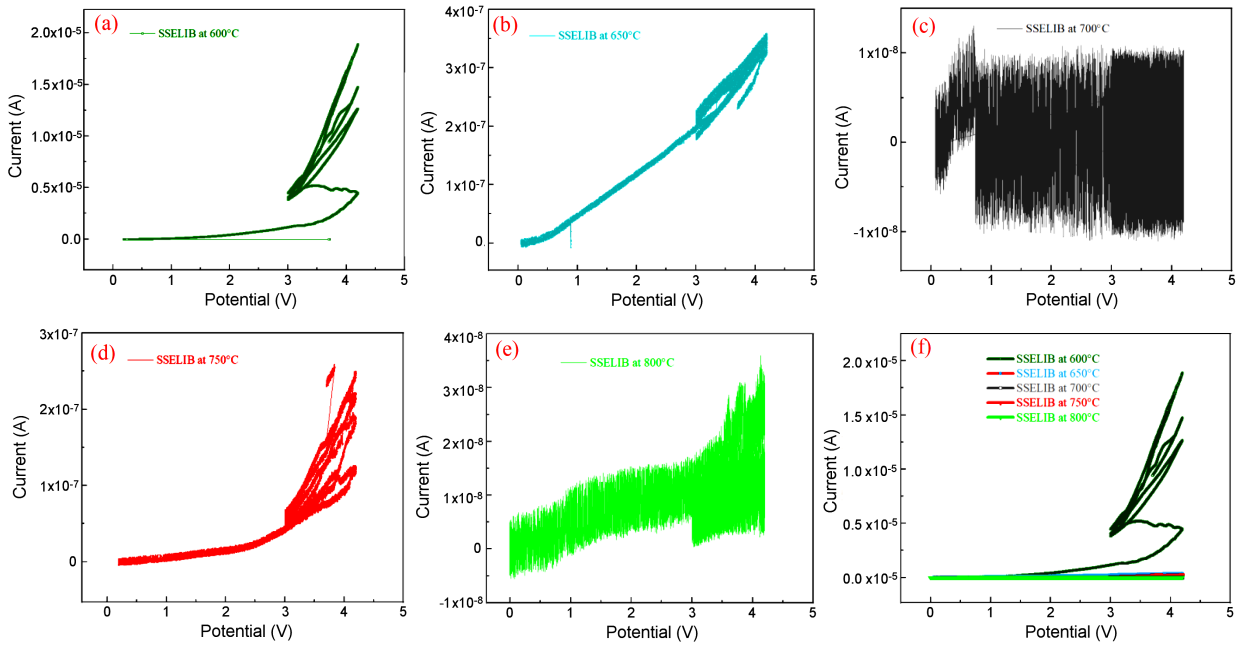

Figure 17. *C-V* graphs of ASSELIB at co-firing temperature of: a) 600 °C/2 h, b) 650 °C/2 h, c) 700 °C/2 h, d) 750 °C/2 h and e) 800 °C/2 h as well as f) combined *C-V* graphs of ASSELIB co-fired at temperatures ranging from 600 to 800 °C

tures in an atmospheric environment. The initial current measured currents for samples sintered at 600 °C/2 h, 650 °C/2 h, 700 °C/2 h, 750 °C/2 h and 800 °C/2 h were 1.910×10^{-5} A (Fig. 17a), 3.610×10^{-7} A (Fig. 17b), 1.210×10^{-8} A (Fig. 17c), 2.610×10^{-7} A (Fig. 17d) and 3.675×10^{-8} A (Fig. 17e), respectively. When combining these results into a single *C-V* plot for the ASSELIB at various co-sintering temperatures (Fig. 17f), only the 600 °C/2 h curve is visible due to the large differences in magnitude. The other curves appear as near-horizontal lines. This result indicates that the sample co-sintered at 600 °C/2 h, with the least dense structure, exhibited the best battery performance, while the samples co-sintered at higher temperatures showed significantly lower performance.

Analysing these results in conjunction with other published research, we believe that lithium ions in the layered NCM structure may be lost in the atmosphere at temperatures above 650 °C/2 h, leading to a substantial reduction in initial current. The negative effects of increased temperature far outweigh any benefits from increased density. According to Kawano *et al.* [43], a co-sintering temperature of 600 °C is optimal for fabricating ASSELIB using tape casting. They suggest a preferable electrolyte layer thickness of 6–9 μm, electrode layer thickness of 15–25 μm and electrode layer density of 0.3 g/cm^2 for both anode and cathode. Although their data serve as a reference, certain concepts align with our findings, such as minimizing electrolyte layer thickness, maintaining thicker anode/cathode layers than the electrolyte and keeping a lower density for electrode layers. Using a lower co-sintering temperature of 600 °C may represent a cost-effective and performance-optimized solution. Interestingly, similar conclusions were reached by Malaki *et al.* [44].

Valorisation

We attempted to use the tape casting method to verify the effectiveness of the pelletizing method. First, we prepared the cathode mixture slurry, electrolyte mixture slurry and anode mixture slurry, then coated these slurries onto thin substrate. After undergoing processes such as drying, laminating, preliminary cutting, vacuum sealing, hydraulic-pressing, precision cutting, debinding, co-firing at the same temperature of 600 °C, grinding and conductive paste coating, the final ASSELIB samples were obtained.

The results obtained from the pelletizing and tape casting methods were very similar. This indicates that if the battery component compositions are properly adjusted, the simple and fast pelletizing method can reliably predict outcomes, saving significant time. However, the main drawback of the pelletizing method is that the solid electrolyte layer is too thick. If a batch of thin electrolyte films can be prepared in advance using the tape casting method and stored properly, then combined with cathode and anode powders for the pelletizing method, more accurate battery data can likely be obtained.

IV. Summary

In this work we successfully fabricated ASSELIB single cells by using a cost-effective and time-saving co-firing method. Compared with the tape casting [45], this approach is quick, convenient and economical. Successful verification of the function and proportional relationships of each raw material in the electrolyte, anode and cathode mixture components was performed. In addition, three key aspects were proposed: i) the development and validation of LABO solder for solid-state

co-firing, ii) the functional expansion and verification of LATP additives and iii) the development and verification of the reduction process for conductive metallic copper in co-firing. These successful experiments are expected to contribute effectively to the industrialization progress of ASSELIB prepared using multi-layer co-firing method [46].

It can be concluded that additional work on optimization of the ASSELIB structure is needed since many important issues still remain unexplored. Future research could focus on interface modification and effective lithium compensation methods during high-temperature co-sintering processes. We look forward to the early practical industrial mass production of the ASSELIB cells to promote the birth of the next generation of batteries.

References

1. TechMax Technical Co,. Ltd., Official website, https://www.techmaxasia.com/knowledge-detail/X-ray-20231211/.
2. T. Ueno, G. Isomichi, T. Masuko, "All-solid-state battery", *United States Patent No. US 20200381774 A1*, 2020.
3. M. Yoshioka, A. Ito, R. Takano, T. Ishikura, "Solid-state electrolyte and all-solid-state battery", *United States Patent No. US 20190006702 A1*, 2019.
4. M. Yoshioka, A. Ito, R. Takano, T. Ishikura, "Solid electrolyte, all solid state battery, method for producing solid electrolyte, and method for producing all solid state battery", *United States Patent No. US 10601073 B2*, 2020.
5. S.-F. Wang, D. Shieh, Y.-A. Ko, Y.-F. Hsu, M.-K. Wu, "Structural and electrical studies of B^{3+}-and-In^{3+}-ion co-doped $Li_{1.3}Al_{0.3}Ti_{1.7}(PO_4)_3$ solid electrolytes", *Solid State Ionics*, **393** (2023) 116174.
6. P. Díaz-Carrasco, A. Duarte-Cárdenas, A. Kuhn, F. García-Alvarado, "Understanding the high performance of nano-sized rutile TiO_2 anode for lithium-ion batteries", *J. Power Sources*, **515** (2021) 230632.
7. Z. Nezamzadeh Ezhyeh, M. Khodaei, F. Torabi, "Review on doping strategy in $Li_4Ti_5O_{12}$ as an anode material for lithium-ion batteries", *Ceram. Int.*, **49** [5] (2023) 7105–7141.
8. A. Chakraborty, S. Kunnikuruvan, M. Dixit, D.T. Mojor, "Review of computational studies of NCM cathode materials for Li-ion batteries", *Isr. J. Chem.*, **60** [8-9] (2020) 850–862.
9. C.-Y. Wu, C.-Q. Feng, C.-F. Zhang, G.-M. Liang, Z.-P. Guo, "Research progress in layered lithium nickel cobalt manganese oxide ternary cathode material", *Battery Bimonthly*, **52** [1] (2022) 3–7.
10. R. Takano, M. Yoshioka, T. Ishikura, A. Ito, "Solid state battery", *United States Patent No. US 20220336807 A1*, 2022.
11. T. Tanaka, T. Tsukada, "All-solid-state battery", *United States Patent No. US 20220416242 A1*, 2022.
12. H. Sato, K. Takeuchi, M. Muroi, T. Masuko, H. Oyake, T. Yano, "All-solid-state lithium ion secondary battery", *United States Patent No. US 20200067133 A1*, 2020.
13. T. Nakamura, H. Suzuki, K. Takeuchi, "Solid electrolyte layer and all-solid-state battery using same", *United States Patent No. US 20220399568 A1*, 2022.
14. R. Takano, Y. Kimura, "Solid-state battery", *United States Patent No. US 20230006200 A1*, 2023.
15. R. Takano, O. Chilagawa, "Solid-state battery", *United States Patent No. US 20230060930 A1*, 2023.
16. T. Masuko, T. Yano, H. Sato, M. Oishi, "All-solid-state secondary battery", *United States Patent No. US 11069898 B2*, 2021.
17. X. Zhu, Xiaobo, S. Zhou, X. Jiang, X. Yao, X. Xu, A. Peng, L. Wang. Q. Xue, "High-performances of $Li_4Ti_5O_{12}$ anodes for lithium-ion batteries via modifying the Cu current collector through magnetron sputtering amorphous carbon", *J. Alloys Compd.*, **830** (2020) 154682.
18. E. Il'ina, S. Pershina, B. Antonov, A. Pankratov, "Impact of Li_3BO_3 addition on solid electrode-solid electrolyte interface in all-solid-state batteries", *Materials*, **14** [22] (2021) 7099.
19. R. Takano, M. Yoshioka, A. Ito, T. Ishikura, "Solid electrolyte and all solid state battery", *United States Patent No. US 20200106131 A1*, 2020.
20. K. Furukawa, T. Fuuruya, "Battery and method of manufacturing the same", *United States Patent No. US 20180123168 A1*, 2018.
21. O. Chikagawa, "Solid-state battery", *United States Patent No. US 20220278365 A1*, 2022.
22. Y. Ren, H. Deng, H. Zhao, Z. Zhou, Z. Wei, "A simple and effective method to prepare dense $Li_{1.3}Al_{0.3}Ti_{1.7}(PO_4)_3$ solid-state electrolyte for lithium-oxygen batteries", *Ionics*, **26** (2020) 6049–6056.
23. K. Kwatek, W. Ślubowska, J. Trébosc, O. Lafon, J.L. Nowiński, "Impact of $Li_{2.9}B_{0.9}S_{0.1}O_{3.1}$ glass additive on the structure and electrical properties of the LATP-based ceramics", *J Alloys Compd.*, **820** (2020) 153072.
24. S.-W. Han, J.H. Ryu, J.Y. Jeong, D.-H. Yoon, "Solid-state synthesis of $Li_4Ti_5O_{12}$ for high power lithium ion battery applications", *J. Alloys Compd.*, **570** (2013) 144–149.
25. J. Shimura, N. Aoki, T. Kato, "Solid-state battery, battery module, and charging method of solid-state battery", *United States Patent No. US 20210066771 A1*, 2021.
26. K. Tanaka, "All-solid-state battery", *United States Patent No. US 12080847 B2*, 2024.
27. M.H. Chu, Z.Y. Huang, T.L. Zhang, R. Wang, T. Shao, C. Wang, W. Zhu, L. He, J. Chen, W. Zhao, Y. Xiao, "Enhancing the electrochemical performance and structural stability of Ni-rich layered cathode materials via dual-site doping", *ACS Appl. Mater. Inter.*, **13** [17] (2021) 19950–19958.
28. Y. Liu, Y. Chen, "Interpretation of cathode material standards for lithium ion batteries", *Energy Storage Sci. Technol.*, **7** [2] (2018) 314–326.
29. P. Yue, Z. Wang, W. Peng, L. Li, W. Chen, H. Guo, X. Li, "Spray-drying synthesized $LiNi_{0.6}Co_{0.2}Mn_{0.2}O_2$ and its electrochemical performance as cathode materials for lithium ion batteries", *Powder Technol.,* **214** [3] (2011) 279–282.
30. T. Hupfer, E.C. Bucharsky, K.G. Schell, M.J. Hoffmann, "Influence of the secondary phase $LiTiOPO_4$ on the properties of $Li_{1+x}Al_xTi_{2-x}(PO_4)_3$ (x = 0; 0.3)", *Solid State Ionics*, **302** (2017) 49–53.
31. K. Shimizu, Y. Tomoshige, A. Baba, "Solid-state battery", *United States Patent No. US 20220140388 A1*, 2022.
32. W. Peng, C. Xu, Z. Li, F. Fan, Q. Zhang, C. Wang, S. Zhong, "Effects of surface density and compaction density on properties of fast charge lithium ion battery", *Nonfer-*

rous Metal Sci. Eng., **8** [3] (2017) 69–73.
33. Y. Tomoshige, M. Nishide, "Solid-state battery", *United States Patent No. US 20220302507 A1*, 2022.
34. M. Kondo, M. Yoshioka. "All solid storage element laminate and battery", *United States Patent No. US 20190363400 A1*, 2019.
35. K. Bando, M. Yoshioka, O. Chikagawa, "Solid-state battery", *United States Patent No. US 20220021024 A1*, 2022.
36. T. Yano, T. Tanaka, T. Masuko, "All-solid lithium ion secondary battery", *United States Patent No. US 20200365935 A1*, 2020.
37. O. Chikagawa, "Solid state battery", *United States Patent No. US 20210296736 A1*, 2021.
38. M. Yoshioka , K. Oshima, "Solid-state battery", *United States Patent No. US 20220285682 A1*, 2022.
39. T. Kawai, M. Otsuka, "Laminated secondary battery and manufacturing method of the same, and device", *United States Patent No. US 20190288342 A1*, 2019.
40. K. Oshima, M. Yohioka, "Manufacturing method of solid state battery and solid state battery", *United States Patent No. US 20220140404 A1*, 2022.
41. N. Iwane, N. Aoki, K. Takahara, Y. Funada, K. Kumagae, K. Shimizu, "Solid state battery", *United States Patent No. US 20220320590 A1*, 2022.
42. K. Kumagae, T. Matsuyama, K. Shimizu, "Solid-state battery", *United States Patent No. US 20220013873 A1*, 2022.
43. Y. Kawano, A. Kato, H. Usui, Y. Domi, H. Sakaguchi, "TiO_2 anode material for all-solid-state battery using NASICON $Li_{1.5}Al_{0.5}Ge_{1.5}(PO_4)_3$ as lithium ion conductor", *Electrochemistry*, **91** [6] (2023) 1344–3542.
44. M. Malaki, A. Pokle, S.-K. Otto, A. Henss, J.P. Beaupain, A. Beyer, J. Müller, B. Butz, K. Wätzig, M. Kusnezoff, J. Janek, K. Volz, "Advanced analytical characterization of interface degradation in Ni-rich NCM cathode co-sintered with LATP solid electrolyte", *ACS Appl. Energy Mater.*, **5** [4] (2022) 4651–4663.
45. R.A. Jonson, E. Yi, F. Shen, M.C. Tucker, "Optimization of tape casting for fabrication of $Li_{6.25}Al_{0.25}La_3Zr_2O_{12}$ sheets", *Energy Fuels*, **35** [10] (2021) 8982–8990.
46. Y. Tomoshige, "Solid-state battery", *United States Patent No. US 20220302498 A1*, 2022.